Journal of Sciences, Islamic Republic of Iran 28(2): 155 - 168 (2017) http://jsciences.ut.ac.ir
University of Tehran, ISSN 1016-1104

High Potash Volcanic Rocks and Pyroclastic Deposits of Damavand Volcano, Iran, an Example of Intraplate Volcanism

M. Mortazavi*

Department of Geology, Faculty of Sciences, University of Hormozgan, P.O.Box 3995, Bandar Abbass, Islamic Republic of Iran

Received: 30 November 2015 / Revised: 4 January 2016 / Accepted: 5 September 2016

Abstract

Damavand is a fascinating dormant stratovolcano, 60 km to the *ENE* of Tehran located in the Alborz Mountains. Damavand volcanic products consist of lava flows and pyroclastic fall, flow and surge deposits from different eruption cycles. The volcanic rocks ranges from trachyandesite to trachyadacite and minor basalt. The mineral assemblage consists of potash feldspar ($Or_{43/7}$), Plagioclase (An_{25} to An_{59}), amphibole, clinopyroxene (augite and salite), orthopyroxene (hypersthene and ferro-hypersthene), biotite (phologophite) and Fe-Ti oxides. Some of the lavas and pyroclastic deposits show calc-alkaline affinities. Lavas from different cycled are classified as shoshonitic types and most pyroclastic deposits are classified as High-K. In comparison to n-type *MORB*, three recent pyroclastic deposits in Damavand show an enrichment in *LREE*, *LILE*, Th, and P and are slightly depleted in *MREE* and *HREE*. Incompatible *LILE* (Rb, Ba and Sr) together with Th and U have not shown broad enrichment as a function of increasing SiO_2 content. Variations in the Major and trace element compositions of Damavand rocks and pyroclastic deposits are difficult to explain by fractional crystallization mechanism. Scatter of several trace elements in plots against SiO_2 and incompatible trace elements, also suggests that the petrogenesis is more complex than a simple fractionation process from a single composition parent. High K, Ba and Rb content in volcanic products could be due to enrichment of these elements in the source. Field observation such as limitation of magmatism in region suggest that decompression melting could be generate the Damavand Lavas and pyroclastic deposits.

Keywords: Damavand Pyroclastics; Damavand Volcano; Damavand lavas.

Introduction

Damavand is a dormant volcano, 60 km to the *ENE* of Tehran, and is the highest mountain (5670 m) in the Middle East and west Asia. Damavand located in the Alborz Mountains of northern Iran in the Mazandaran Province. Damavand is the largest strata-volcano of the calcalkaline and is an outstanding location to

* Corresponding author: Tel:+989173616592; Fax: +987633711027; Email:hsm_mortazavi@yahoo.co.uk, Mohsen.mortazavi@hormozgan.ac.ir

investigate volcanic and magmatic processes. There are no known historic eruptions of Damavand and the latest eruption occurred 7000 years ago. Damavand volcanic products consist of many lava flows and pyroclastic fall, flow and surge deposits which cover an area up to 400 km^2 around the volcano. Although the stratigraphy, geochronology, volcanology and petrology of the Damavand volcano has been studied by researches, but need to study more extensive. Damavand history include several eruptions of intermediate lavas and widespread pyroclastic deposits which can be interpreted as a powerful explosive volcano.

The purpose of this article is to report the petrology, mineral chemistry, and geochemistry of lavas and pyroclastic deposits to provide information on the genesis of magmas. Damavand volcanic rocks and pyroclastic deposits have investigated. Petrology, geochemistry and mineral chemistry of 40 volcanic rocks have been studied and geochemistry of more than 90 pumice samples from three recent explosive eruptions also examined. These eruptions from older to younger were named Rayneh Pyroclastic Deposits, Karam-Poshteh Pyroclastic Deposits and Mallar Pyroclastic Deposits [Fig.1a,b,c and d] [11]. Geochemical similarities between the lavas and pyroclastic deposits were also documented.

Geological background

Volcanism on Damavand goes back to at least 1 ma with on older sequence (Old Damavand) and younger sequence (Young Damavand). The youngest known eruption is a lava flow on the western flanks with an age of 7.3 ka[4]. Damavand lavas ranges from basalt (as early stage of volcanism) to dacite but being predominantly trachyandesite. The phenocrysts are set in a fine grained intergranular to intersertal groundmass and they typically show porphyritic to glomero-porphyritic texture.

Trace element geochemistry has affinities with intraplate volcanism rather than subduction-related volcanism. The tectonic setting of Damavand is puzzling. It is located in a young and very active zone of compression and strike-slip faulting. Deep thrust faults border the mountain range with large strike-slip faults towards the centre and south [8, 16].Volcanoes located in regions of compressional thrust faulting are uncommon, although there are some rare examples *e.g.* [6].

Allenbach (1963; 1970) [1, 2] was the first

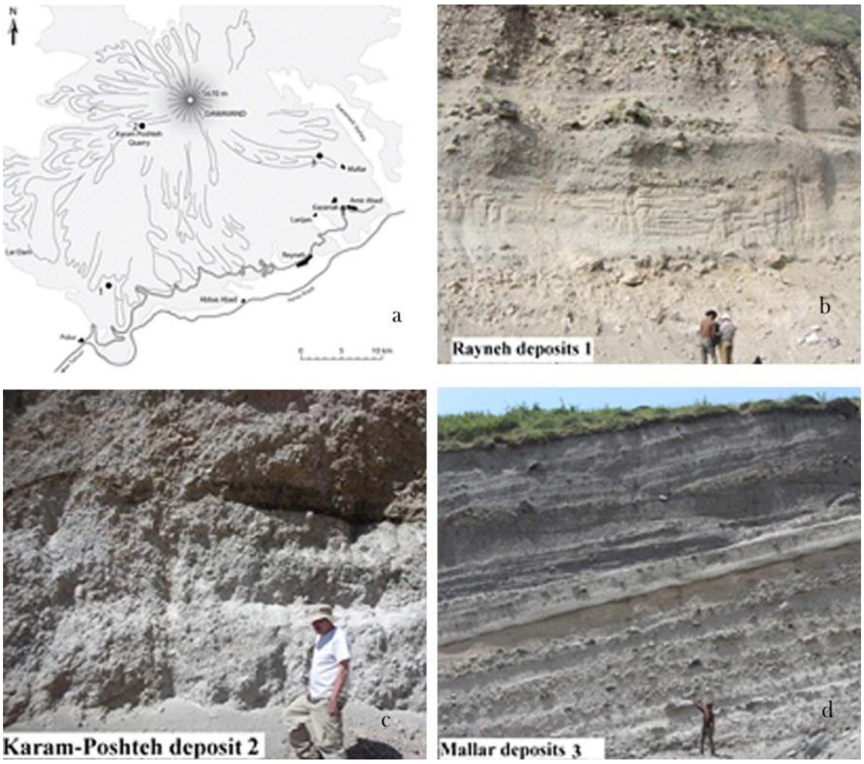

Figure 1. (a) Outline of Damavand Volcano, major villages and geographic features [12]. Numbers 1, 2, and 3 in the map show a section of Rayneh, Karam-Poshteh and Mallar pyroclasytic deposits recpectively.(b,c,and d), locations of pyroclastic samples studied in this paper.

systematic study of the geology. Knowledge about the stratigraphy, age and geochemistry was significantly enhanced by the study of*Davidson et al. (2004)* [4], *Mortazavi et al. (2009*) [12] and *Mortazavi (2013)*) [13]. There is, however, no detailed or reliable geological map. The youngest known eruption is a lava flow on the western flanks with an age of 7.3 ka. *Davidson et al. (2004)* [4] also confirmed that the largely volcanic products are remarkably uniform in composition and petrology, being predominantly porphyritic trachyandesite. *Darvishzadeh and Mordi (1997)* [3] described young pyroclastic deposits that they concluded were formed by sub-Plinian explosive eruptions. *Mortazavi et al. (2009)* [12] describe the distribution and characteristics of three pyroclastic units and interpret the, in terms of eruption style, likely magnitude, and hazardous effects. *Mortazavi et al. (2009*) [12] then discuss the current state of the volcano and the likelihood of the next eruption being explosive. He discuss possible scenarios and impacts of future eruptions locally and regionally and present the hazards that would result from tephra fall in the cities and provinces neighboring Damavand. *Mortazavi et al. (2009)* [11] show that Damavand volcano has had high intensity explosive eruptions, producing widespread pyroclastic fall and flow deposits. Mohammadi (2016) investigate the geochemistry and petrogenesis of the youngest lavas of Damavand and suggest that volcanic rocks originated from adakitic magma [11]. Mineralogy and geochemistry of lavas and pyroclastic deposits can provide valuable information about evolution of magma through time and composition of parent magmas. To achieve this goal, field relationships and geological features, texture, petrology, geochemistry, and petrogenesis of lava and pyroclastic deposits will be described.

Petrography

The petrography, crystal chemistry, petrology and geochemistry of volcanic and pyroclastic rocks in Damavand volcano are described. We adopt a classification, modified from *Gill (1981)* [7], and based on dry analysis: basalt (<53% SiO_2); andesite (53-63% SiO_2); dacite (63-68% SiO_2); rhyodacite (68-72% SiO_2) and rhyolite (> 72% SiO_2). Description of crystal grain sizes are in terms of: phenocrysts, microphenocrysts and microlites. In the following account microphenocrysts and microlites are considered as components of the groundmass in those rocks with porphyritic texture. The volume percent of crystal phases was determined in thin sections under optical microscope using x_{40} magnification. Mineral analyses were performed on a *JEOL JXA* 8600 four spectrometer electron probe with operating conditions of 15 *KV*, beam current of 15 Na and minimum beam diameter of 1 nm. Mineral analyses are provided in the electronic supplementary material.

The volcanic rocks ranges from trachyandesite to trachydacite (SiO_2 53-65%) [Fig. 2]. Although basalt (SiO_2 45%) are available as minor. The mineral assemblage consists of potash feldspar (*kf*), plagioclase (*pl*), amphibole (*amp*), clinopyroxene (*cpx*), orthopyroxene (*opx*), biotite (*biot*) and Fe-Ti oxide (*opq*). There are also minor interstitial glass and vesicles. In the following description we distinguish between large crystals, small crystals and crystallites using an arbitrary division of maximum crystal length (> 300 µm, 300-100 µm and < 100 µm).

Potash feldspar is commonly the most abundant of

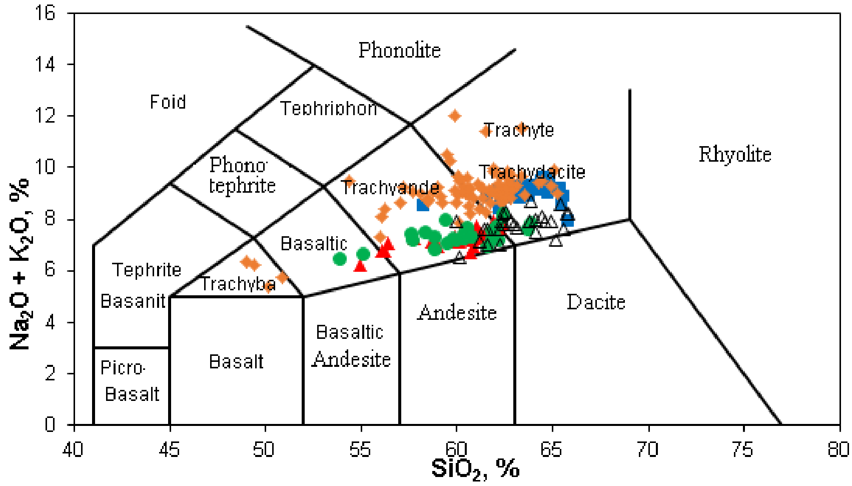

Figure 2. Na_2O+K_2O versus SiO_2 diagram showing volcanic rocks and pyroclastic deposits ranges from trachyandesite to trachydacite.

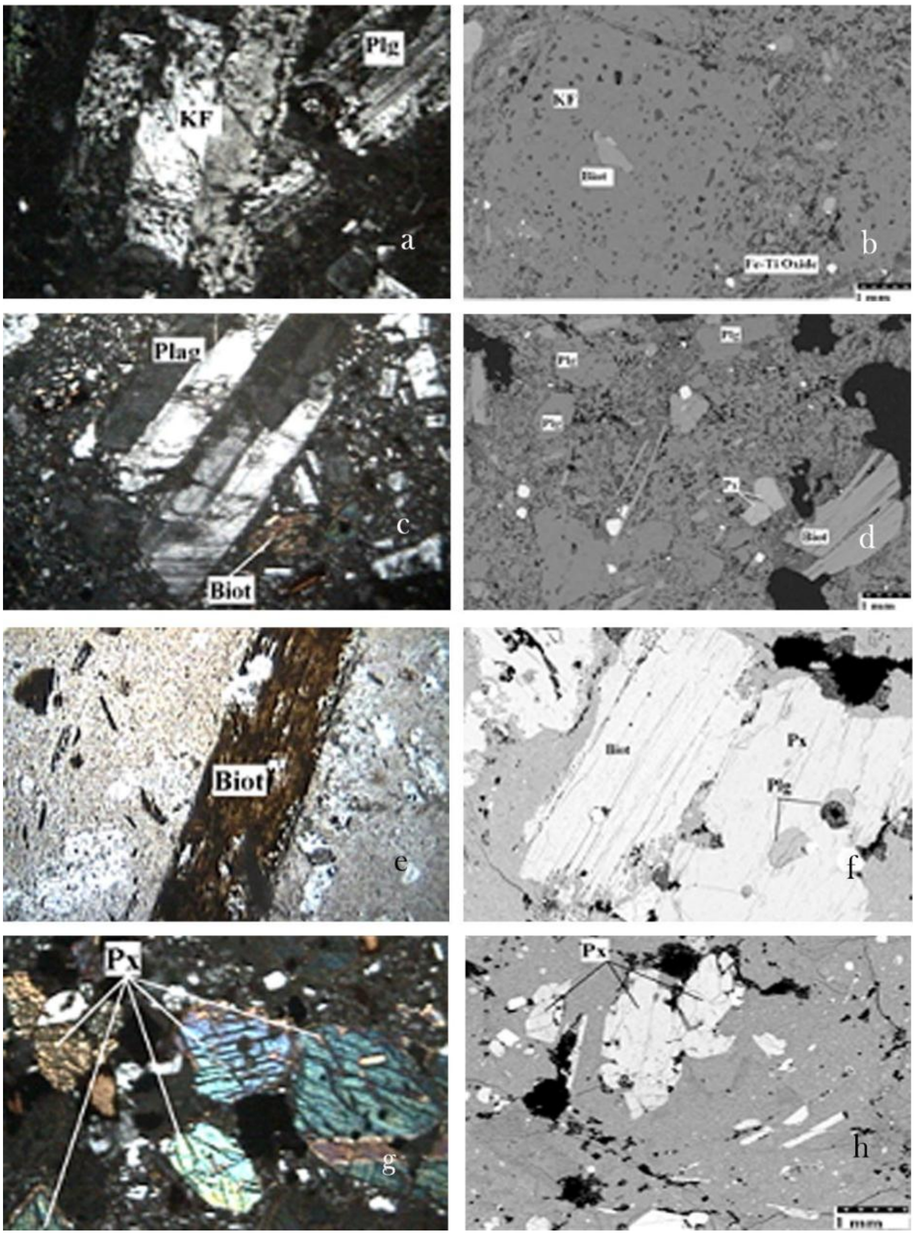

Figure 3. Trachyandesite (63% SiO_2) show (a): potash feldspar with sieve texture and Carlsbad twining. (b): SEM image of Potash feldspar.Biotite and Fe-Ti oxide are present as inclusions. (c): Plagioclase with polysenthetic twining. Biotite and pyroxene occurs as mafic phase microphenocrysts.(d): SEM image of Plagioclase, Biotite and Fe-Ti oxide are present as inclusions. (e): Biotite phenocrysts and microphenocrysts in trachyandesits, Plagioclase and pyroxene occurs as mafic phase microphenocrysts. (f): *SEM* image of biotite, Pyroxene, plagioclase and Fe-Ti oxide as inclusions. (g): Euhedral pyroxene phenocrysts and microphenocrysts. Some crystals show two cleavage trace, one parallel to (1-1 0) and the other parallel to 110 plane. (h): *SEM* image of pyroxene, in trachyandesite.Mag: 40x, cpl light, *KF*; potash feldspar,*Biot*: Biotite, *Plg*: plagioclase and *PX*: Pyroxene.*Plg*: Plagioclase.

the large crystals (30%) in most Damavand volcanic rocks. Potash feldspar also occurs as small crystals and crystallites. Most large crystals are subhedral to unhedral; some are tabular show sieve texture and rarely contain inclusions of brown glass, Fe-Ti oxides and apatite. Crystal size ranges from 0.7 to 2.2 and maximum crystal size rich to 3 mm. Potash feldspar phenocrysts are divided into zoned and unzoned crystals. Carlsbad twining is common and reaction rim also occur in some crystals [Fig. 3a and b]. Potash content (Or from K_2O + Na_2O + CaO)in majority of large potash feldspar rich to 43/7% [Table 1].

Plagioclase is occurs as phenocrysts and microphenocrysts. Plagioclase also occurs as small crystals and crystallites. Plagioclase abundance is between 5 to 10 percent. Crystal size ranges from 0.7 to

2.2 and maximum crystal size rich to 3 mm. Most large crystals are euhedral to subhedral and prismatic and rarely unhedral; some are tabular. Plagioclase commonly show polysynthetic and albitic twining and commonly contain inclusions of Fe-Ti oxides. Plagioclase phenocrysts are divided into zoned and unzoned crystals [Fig. 3c & d]. An content (Ca from K_2O + Na_2O + CaO)in majority of large plagioclase ranges from An_{25} to An_{59} [Table 1].

Biotite is occurs almost as microphenocrysts but rarely phenocrysts. Biotite also present in groundmass. Biotite abundance is between 5 to 10 percent. Crystal size is commonly less than 1mm but in some cases crystals with 2 mm long can be seen. Most crystals are subhedral and show perfect cleavage. Parallel extinction and brownish pelochroism are their main character. Biotite in many cases altered to opaque crystals. A framework of crystals can be distinguish in progressive alteration. Routile and apatite occur as inclusions in Biotite [Fig. 3e&f]. Microprobe analyses [Table1] show that biotite are rich in Fe-Ti suggest that alteration to Fe-Ti Oxides. Microprobe data suggest most micas are phologophite.

Clinopyroxene and orthopyroxene (cpx>>opx) occur as subhedral to unhedral crystals with maximum length of 1 mm and width of 0.8 mm. Individual crystals are either unzoned or show normal zoning with higher Fe/Mg rims. Pyroxenes contain abundant inclusions of glass, needles of apatite and Fe-Ti oxides [Fig. 3g&h], [Table 1].

Pyroxene content varies between less than 5% to 7 %. Clinopyroxene (En $_{(38-46)}$-Fs $_{(4-12)}$-Wo $_{(44-53)}$ to En_{46}-Fs_{13}-Wo_{40}) mostly classified as augite and salite with a few cases plotting as endiopside and diopside. Most orthopyroxene are hypersthene (En_{50} to En_{57}) with Ca less than 0.5. There are also a few ferro-hypersthene crystals [Table 1].

The matrix of the trachyandesitic rocks (18-30%) is typically very fine grained with microcrystalline and crystallites of plagioclase, k-feldspar, clino and ortho pyroxene, apatite, opaque minerals, secondary calcite and rarely glass. Vesicles up to 2.5 mm in width are

Table 1. Representative microprobe analyses of biotite, K feldspar, Pyroxene, Fe oxides and apatite from Damavand volcanic rocks.

	Biot	**Biot**	**Biot**	**Biot**	**Biot**	**Biot**
Ideal Cations	7.82	7.82	7.82	7.82	7.82	7.82
Ideal Oxygens	11.00	11.00	11.00	11.00	11.00	11.00
SiO2	38.08	38.09	39.26	36.72	37.41	37.69
TiO2	5.38	5.30	5.51	5.96	6.18	6.03
Al2O3	13.05	12.90	13.40	13.32	13.14	13.20
Cr2O3	0.02	0.03	0.01	0.00	0.02	0.01
FeO	11.87	11.50	11.35	11.38	12.62	13.02
MnO	0.06	0.07	0.06	0.04	0.10	0.07
MgO	16.81	16.64	15.11	16.31	15.54	16.03
Na2O	0.75	0.95	0.85	0.97	0.99	0.90
K2O	8.55	8.67	8.40	8.32	8.52	8.93
Total	94.57	94.15	93.97	93.00	94.51	95.90

Table 1. Cntd

	Px	**Px**	**Px**	**Px**	**Px**	**Px**	**Px**	**Px**	**Px**	**Px**	**Px**	**Px**	**Px**
Ideal Cations	4.00	4.00	4.00	4.00	4.00	4.00	4.00	4.00	4.00	4.00	4.00	4.00	4.00
Ideal Oxygens	6.00	6.00	6.00	6.00	6.00	6.00	6.00	6.00	6.00	6.00	6.00	6.00	6.00
SiO2	53.38	51.89	53.78	52.86	52.46	52.51	68.43	50.93	48.32	46.97	51.68	48.67	46.07
TiO2	0.24	0.74	0.39	0.40	0.50	0.24	0.42	0.96	0.79	0.98	0.33	0.68	0.93
Al2O3	0.82	2.07	1.25	1.22	2.23	1.04	14.37	3.53	5.37	6.84	2.29	4.89	7.66
Cr2O3	0.00	0.21	0.04	0.11	0.23	0.00	0.01	0.16	0.00	0.00	0.25	0.00	0.01
FeO	7.69	7.56	7.00	7.50	6.75	8.53	2.37	6.27	8.00	8.75	5.35	7.89	8.98
MnO	0.48	0.28	0.29	0.39	0.25	0.44	0.08	0.10	0.17	0.20	0.10	0.26	0.24
MgO	14.82	14.96	15.72	15.33	15.33	14.77	0.31	14.87	12.98	11.79	15.91	12.65	11.29
CaO	22.17	21.51	21.64	21.47	21.39	21.13	1.07	21.57	23.35	22.92	23.63	23.07	22.88
Na2O	0.47	0.54	0.47	0.64	0.57	0.62	4.36	0.46	0.36	0.40	0.19	0.63	0.57
Total	100.08	99.77	100.59	99.93	99.72	99.28	96.70	98.85	99.33	98.86	99.74	98.75	98.63
En	43.06	44.56	45.06	45.41	45.36	44.12	1.22	44.56	40.86	38.22	46.43	40.56	37.94
Fs	10.66	9.41	10.36	8.88	9.16	10.51	95.78	9	6.32	8.40	4	6.28	6.77
Wo	46.28	46.03	44.58	45.70	45.49	45.37	46.44	46.44	52.83	53.38	49.57	53.16	55.29

Table 1. Cntd

	Plg	**Plg**	**Plg**	**Plg**	**Plg**	**Plg**	**Plg**	**Plg**	**Plg**	**Plg**
Ideal Cations	4.91	4.91	4.91	4.91	4.91	4.91	4.91	4.91	4.91	4.91
Ideal Oxygens	8.00	8.00	8.00	8.00	8.00	8.00	8.00	8.00	8.00	8.00
SiO2	62.95	60.26	61.69	60.57	61.98	61.97	60.34	31.37	35.68	59.68
	Plg	Plg	Plg	Plg	Plg	Plg	Plg	Plg	Plg	Plg
TiO2	0.12	0.04	0.03	0.04	0.05	0.03	0.04	0.04	0.03	0.06
Al2O3	23.32	24.81	24.31	24.37	25.35	23.69	25.07	13.69	15.77	24.58
FeO	0.74	0.47	0.41	0.43	0.47	0.38	0.28	0.52	0.48	0.46
MnO	0.02	0.00	0.01	0.00	0.01	0.02	0.00	0.04	0.02	0.02
MgO	0.08	0.01	0.05	0.01	0.03	0.02	0.02	0.08	0.10	0.02
ZnO	0.00	0.00	0.00	0.00	0.00	0.00	0.00	0.00	0.00	0.00
CaO	5.09	6.42	5.69	6.00	6.35	4.87	6.76	5.85	5.96	6.30
	Plg	Plg	Plg	Plg	Plg	Plg	Plg	Plg	Plg	Plg
Na2O	6.93	7.06	7.71	7.20	6.77	7.97	6.84	8.80	9.48	7.42
K2O	2.18	1.08	1.35	1.24	1.14	1.57	1.01	0.70	0.66	1.10
Total	101.44	100.13	101.23	99.85	102.15	100.53	100.37	61.09	68.18	99.63
Ab	62.03	62.39	65.68	63.54	61.40	68.17	60.84	70.45	71.77	63.83
An	25.14	31.35	26.77	29.27	31.82	22.99	33.23	22.89	24.93	29.96
Or	12.82	6.26	7.55	7.18	6.78	8.84	5.93	3.66	3.30	6.22

Table 1. Cntd

	Plg	**Plg**	**Plg**	**Plg**	**Kf**	**Kf**	**Kf**	**Kf**	**Kf**	**Kf**
Ideal Cations	4.91	4.91	4.91	4.91	4.91	4.91	4.91	4.91	4.91	4.91
Ideal Oxygens	8.00	8.00	8.00	8.00	8.00	8.00	8.00	8.00	8.00	8.00
SiO2	54.68	58.68	50.80	49.33	58.70	59.38	59.38	68.29	36.07	36.07
TiO2	0.06	0.02	0.46	0.06	0.07	0.04	0.05	0.66	0.34	0.34
Al2O3	27.51	16.23	17.01	19.63	25.47	24.89	24.81	15.53	9.48	9.48
FeO	0.41	0.28	1.11	0.31	0.50	0.48	0.47	2.03	1.49	1.49
MnO	0.01	0.03	0.00	0.01	0.00	0.01	0.02	0.03	0.03	0.03
MgO	0.01	0.29	0.03	0.01	0.04	0.01	0.01	0.24	0.45	0.45
	Plg	Plg	Plg	Plg	Kf	Kf	Kf	Kf	Kf	Kf
CaO	10.02	4.31	2.51	4.70	7.43	6.68	6.84	0.84	0.69	0.69
Na2O	5.28	5.82	6.42	6.23	6.58	7.23	7.10	4.81	2.90	2.90
K2O	0.61	2.26	1.46	0.86	0.97	1.01	1.06	6.23	3.47	3.47
Total	98.61	87.95	79.81	81.18	99.77	99.73	99.74	98.68	54.93	54.93
Ab	47.07	60.07	73.22	66.33	58.10	62.38	61.34	51.34	52.07	52.07
An	49.36	24.57	15.84	27.66	36.26	31.88	32.66	4.94	6.88	6.88
Or	3.57	15.35	10.94	6	5.64	5.75	6	43.71	41.06	41.06

	Fe-Ox	**Fe-Ox**		**Apat**	**Apat**	**Apat**	**Apat**	**Apat**	**Apat**	**Apat**
Ideal Cations	1.00	1.00								
Ideal Oxygens	1.50	1.50	SiO2	0.42	0.38	0.45	0.30	0.28	0.43	0.67
			TiO2	0.00	0.00	0.03	0.00	0.00	0.00	0.02
SiO2	0.08	0.09	Al2O3	0.00	0.01	0.02	0.02	0.01	0.01	0.00
TiO2	4.54	3.85	Cr2O3	0.00	0.00	0.00	0.00	0.00	0.00	0.00
Al2O3	3.45	2.75	FeO	0.21	0.27	0.70	0.34	0.30	0.50	0.27
	Fe-Ox	Fe-Ox		Apat	Apat	Apat	Apat	Apat	Apat	Apat
Cr2O3	0.18	0.16	MnO	0.04	0.10	0.10	0.13	0.09	0.08	0.04
FeO	80.69	81.19	MgO	0.15	0.28	0.50	0.33	0.29	0.29	0.12
MnO	0.57	0.56	ZnO	0.00	0.00	0.00	0.00	0.00	0.00	0.00
MgO	3.77	3.35	CaO	49.07	52.36	52.42	52.92	52.91	52.19	49.84
ZnO	0.00	0.00	Na2O	0.30	0.37	0.60	0.57	0.49	0.52	0.20
CaO	0.02	0.05	K2O	0.01	0.00	0.08	0.00	0.02	0.07	0.02
Na2O	0.07	0.06	Total	50.20	53.76	54.89	54.61	54.40	54.08	51.19
K2O	0.00	0.05								

rarely present. The matrix fills the spaces between the interlocking frameworks of large crystals. Rocks characteristically display porphyritic texture. In some cases seriate texture is shown by a wide range of grain sizes of plagioclase, pyroxene and small proportions of Fe-Ti oxide. In some samples the wedge-shaped intersections between the large and small crystals have occupied by hypo-crystalline material.

Geochemistry trends

The identification of the geochemical affinities of pyroclastic rocks was carried out using oxide wt% to plot on the triangular AFM diagram. Majority pyroclastic deposits plot just below and minor on the boundary line and therefore show calc-alkaline affinities in this diagram [Fig. 5].

The wt% oxide data are also plotted in FeO/MgO

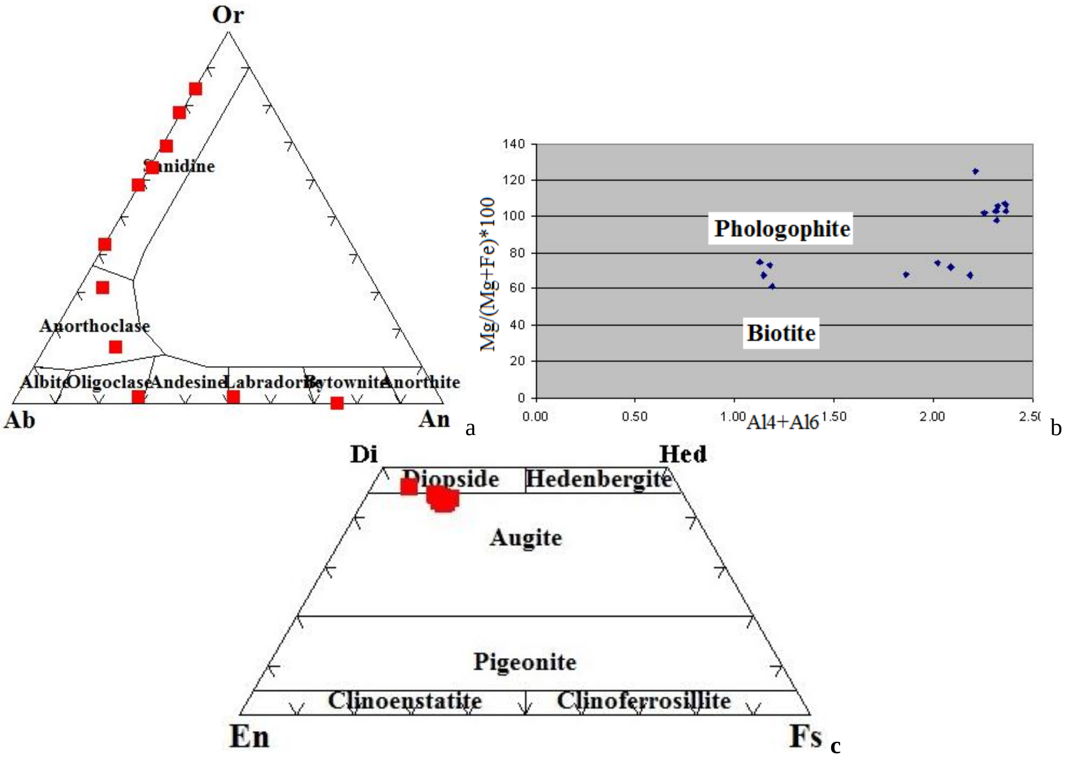

Figure 4. (a): Composition of potash feldspar and plagioclase in volcanic rocks. There are wide ranges of potash feldspar and plagioclase in volcanic rocks. (b): Micas are almost phologophite in Damavand volcanic rocks and Fe-Ti content result of biotite alteration. (c): Pyroxenes in Damavand volcanic rocks are rich in Ca and poor in Fe and mainly are diopside.

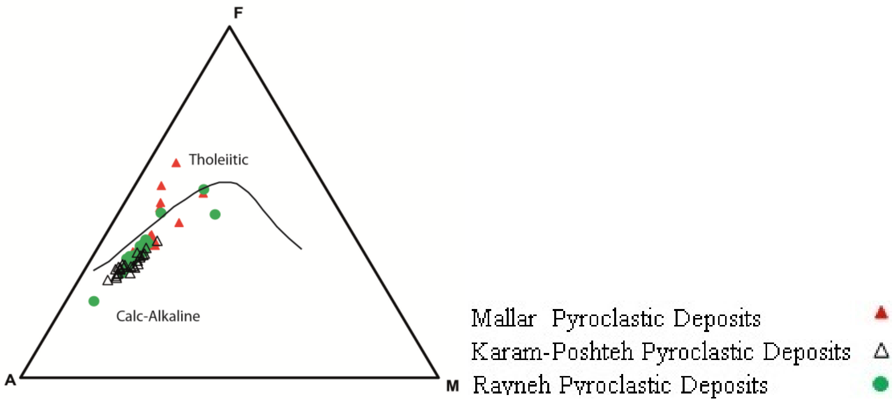

Figure 5. AFM diagram. P deposits plot just below and or on the boundary line in the calc-alkaline part of diagram. Mallar pyroclastic deposits (solid triangles), Karam-Poshteh pyroclastic deposits (open triangles) and Rayneh pyroclastic deposits (solid circles).

versus SiO_2 diagram [Fig. 6]. Most pyroclastic deposits show tholeiitic affinities.

It is noted that some samples plot within the calcalkaline field in the AFM diagram [Fig. 5], but plot within the tholeiitic field in the Miyashiro diagram [Fig.6]. This is simply an artifact of the different arbitrary boundaries between these igneous suites on the two different diagrams. It also reflects the fact that these samples have compositions close to the boundaries and also due to presence of Fe-Ti oxides.

Based on a K_2O versus SiO_2 diagram [Fig. 7a], with classification boundaries after *Peccerillo and Taylor (1976)*[15], lavas from different cycled are classified as shoshonitic types. Most pyroclastic deposits are classified as High-K. It is clear from this diagram [Fig. 7a] that lava and pyroclastic deposits define trends from generally “high-K” to “shoshonitic series” with increasing SiO_2 content. The key point is that the K_2O

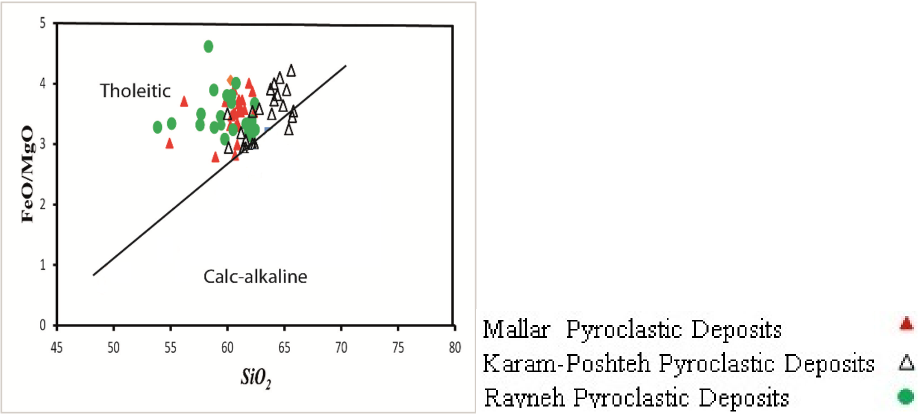

Figure 6. FeO/MgO vs. SiO_2 diagram for pyroclastic deposits. Pyroclastic deposits plotted in tholeiitic field. The line defining the boundary between the fields of tholeiitic and calc-alkaline volcanic suites after [10] is shown for reference. Mallar pyroclastic deposits (solid triangles), Karam-Poshteh pyroclastic deposits (open triangles) and Rayneh pyroclastic deposits (solid circles).

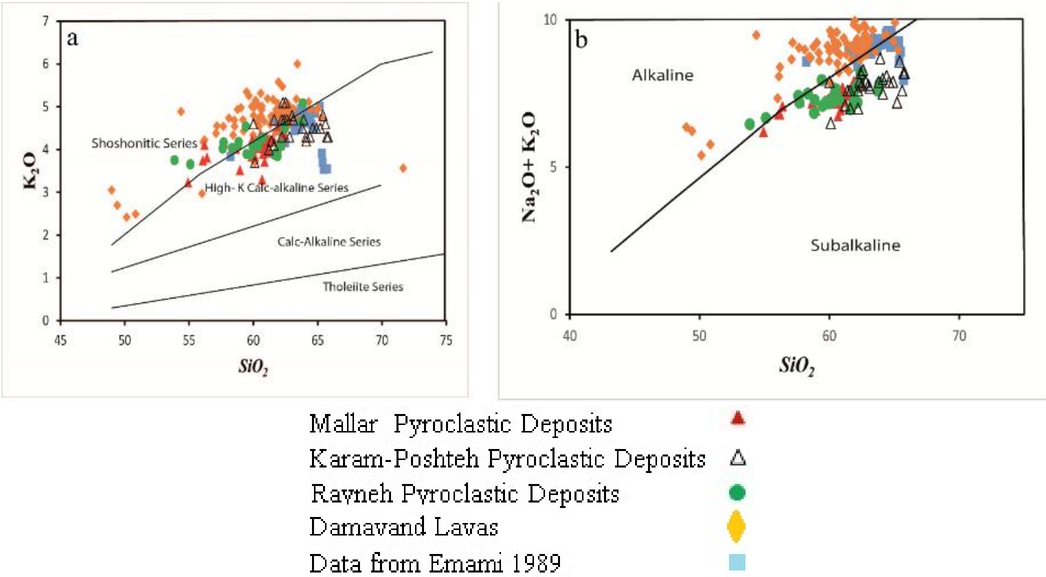

Figure 7. (a): K_2O versus SiO_2 diagram, modified after [16] showing thrachyandesitic rocks and pyroclastic deposits from this study. (b): Na_2O+K_2O diagram versus SiO_2, showing thrachyandesitic rocks and pyroclastic deposits from this study.Mallar pyroclastic deposits (open triangles), Karam-Poshteh pyroclastic deposits (open triangles) and Rayneh pyroclastic deposits (solid circles), Damavand lavas (solid diamond) and Damavand lavas data from [5] (solid square).

content will be decrease from older deposits (Rayneh pyroclastic deposits) to younger ones (Mallar pyroclastic deposits). Na_2O+ K_2O diagram versus SiO_2 also show that Damavand lavas are alkaline whilst pyroclastic deposits almost plotted in sub-alkaline area [Fig.7b].

Major element geochemistry

Major element variation diagrams for Damavand lavas and pyroclastic deposits rocks are shown in [Fig. 8]. K_2O in Damavand pyroclastic deposits shows a flat or weak tendency to decrease with increasing SiO_2 between 60 to 65 wt%, whilst K_2O in Damavand lavas increases with increasing SiO_2. Some of the volcanic rocks and the pyroclastic deposits are distinctive on the K_2O versus SiO_2 diagram [Fig. 8] in having lower K_2O values at a given content SiO_2 in comparison to other volcanic rocks and the pyroclastic deposits. It found that the pyroclastic deposits on Damavand decreased in relative K_2O content with time and the older pyroclastic deposits being richer in K_2O. It is also observed that the

K_2O content are not the same in different volcanic rocks on Damavand. CaO content in lavas, show considerable decrease with increasing SiO_2 and scatter or weak tendency in Karam-Poshteh Pyroclastic deposits. Taken together, CaO content in lavas, Rayneh and Mallar pyroclastic deposits, show linear trends and decrease with increasing SiO_2. Al_2O_3 in volcanic rocks shows a slight decrease in SiO_2 between 55 to 65wt%,

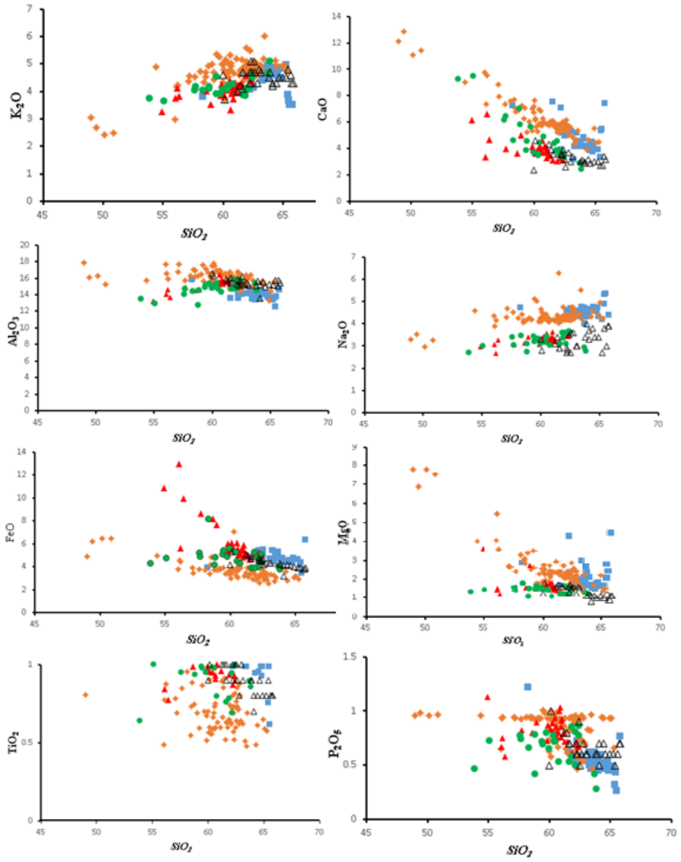

Figure 8. Major elements variation diagrams for lavas and pyroclastic deposits of Damavand Volcano. Symbols are the same as Fig.7.

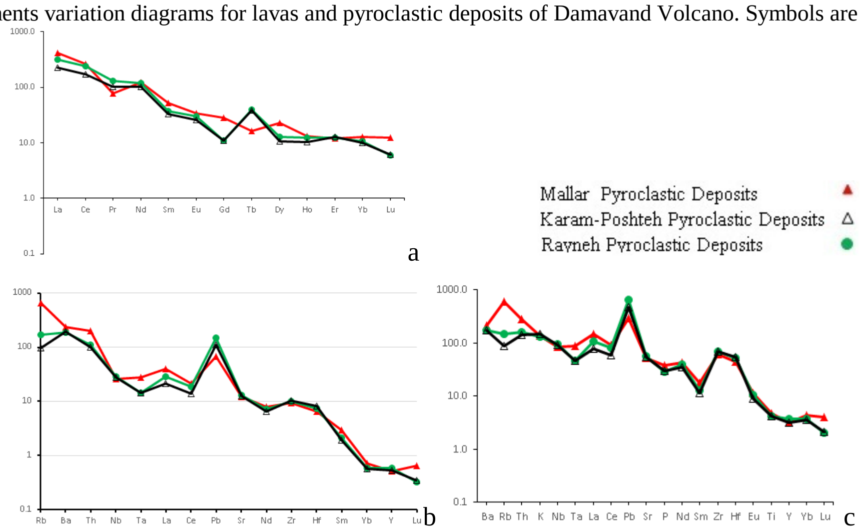

Figure 9. Multi element diagrams for (a): rare earth elements. Data normalized to N-type *MORB.* and (b) trace elements arranged in an order of increasing incompatibility and mobility from right to left normalized to *N-type MORB* (b) and primitive mantle (c). Each line in the diagrams, (graph) is an averages compositins of 30 Samples.

whereas Al_2O_3 in pyroclastic deposits from the other units (Rayneh, Karam-Poshteh and Mallar) show a linear trend with increasing SiO_2. Na_2O shows a linear trend in both volcanic and pyroclastic deposits, but are notable for having significantly lower content in pyroclastic deposits compare with volcanic rocks. FeO content in volcanic and pyroclastic deposits show a linear trend and slight decrease with increasing SiO_2. Several Pyroclastic samples shows significantly higher FeO than the majority. MgO in pyroclastic deposits remains approximately constant over a range of SiO2 (55-65%), except for higher amount in volcanic rocks which show a decrease in MgO continuously with increasing SiO_2. Pyroclastic deposits have higher FeO and lower MgO than volcanic rocks.TiO_2 shows considerable scatter in both volcanic rocks and pyroclastic deposits. Although P_2O_5 has a scattered trend in both volcanic rocks and pyroclastic deposits, it generally shows a flat variation with SiO_2 [Fig. 8] [Table 2].

race element geochemistry

The trace element characteristics of the volcanic rocks and pyroclastic deposits in Damavand Volcano are displayed using the multi element spider diagram of *Pearce (1982)* [14], in which elements are normalized against a *N-type MORB* standard *Sun and McDonough, (1989)* [17]. The trace element data have been plotted in terms of Rare Earth Elements (*REE*) alone [Fig. 9a] and for selected trace elements, after consideration of relative incompatibilities and mobility [Fig. 9 b & c] [Table 3]. Here light, middle and heavy rare earth elements are denoted as *LREE*, *MREE* and *HREE* respectively and Large Ion Lithophile Elements as *LILE*. To avoid from any complexity (90 samples) and ability to compare trace elements from different eruptive phase, the averages of elements in each eruptive phases have been plotted.

In comparison to *N-type MORB*, three recent pyroclastic deposits in Damavand show an enrichment in *LREE* (La, Ce, Sm, Eu), *LILE* (Ba, Rb, K, Sr,), Th, U, and P and are slightly depleted in *MREE* (Gd, Tb,

Table 2. Representative major and trace elementdata of volcanic rocks and pyroclastic deposits from Damavand volcano.

Sample	1-D	2-D	3-D	4-D	5-D	6-D	7-D	8-D	9-D	S3L8C	S3L8M	S3L8F	S3L6L
SiO2	63.5	64.75	63.56	58.21	62.47	62.46	63.38	65.17	64	57.74	61.00	61.51	61.03
TiO2	1.04	0.93	1.05	1.79	1.15	1.16	1.1	1.6	1.15	1.12	1.06	1.01	1.08
Al2O3	14.42	14.12	14.37	15.91	14.25	14.13	14.41	13.5	13.6	14.93	15.45	15.24	15.55
FeO	4.93	4.43	4.84	3.97	5.59	5.03	4.71	4.7	4.76	8.64	4.85	4.63	5.87
MnO	0.07	0.07	0.08	0.09	0.08	0.07	0.07	0.07	0.07	<.1	<.1	<.1	0.10
MgO	1.68	1.7	1.79	2.9	1.99	1.95	1.85	1.73	1.67	1.49	1.38	1.30	1.60
CaO	4.46	3.8	4.63	7.31	5	5.05	4.61	3.96	4.91	3.96	3.27	3.15	4.04
Na2O	4.5	4.74	4.57	4.75	4.71	4.46	4.8	4.24	4.36	3.96	3.27	3.15	4.04
K2O	4.82	4.9	4.5	3.84	4.17	4.71	4.54	5.01	4.89	3.07	3.20	3.17	3.63
P2O5	0.58	0.55	0.6	1.23	0.59	0.59	0.52	0.5	0.6	4.16	4.16	4.26	4.05
Total	100	100	100	100	100	100	100	100	100	0.82	0.76	0.71	0.93
Ba	1189	1080	1153	1289	1132	1132	1148	1196	1141	100.00	100.00	100.00	100.00
Rb	110	139	111	61	99	107	104	112	109	330.25	398.15	365.80	395.00
Sr	1172	1052	1254	1676	1282	1315	1284	1434	1343	1082.2	1206.6	1128.79	1198.7
Zr	316	341	305	332	304	298	294	321	303	610.19	753.79	764.85	755.50
Pb	18	26	27	26	36	17	17	19	14	34.47	22.03	8.61	31.81
Y	19	20	18	16	18	1	817	19	18	12.70	15.52	13.31	16.14
Nb	43	47	48	58	45	45	35	47	37	46	46	49	48.79
U	2	5	0	0	0	0	0	0	2	2	6	3	4.09
Th	18	32	21	10	19	17	16	19	15	21	24	22	23.93

Sample	S3L9A	S3L12C	S3L12M	S3L12F	S3L16C	S3L16M	PR2	PR3	PR4	PR5	PR6
SiO2	60.87	61.90	62.20	56.39	62.34	62.39	65.80	62.40	60.00	62.60	62.80
TiO2	1.13	0.93	0.87	0.77	0.93	0.90	0.80	1.00	0.90	0.90	0.80
Al2O3	15.53	15.16	15.05	13.67	15.29	15.16	15.40	15.60	16.60	16.20	15.30
FeO	5.50	5.13	5.21	9.97	4.88	5.01	3.90	4.50	4.20	4.20	4.30
MnO	<.1	<.1	<.1	0.30	<.1	<.1	<.1	<.1	3.50	<.1	<.1
MgO	1.84	1.28	1.35	1.16	1.39	1.36	1.10	1.50	1.20	1.60	1.20
CaO	4.15	3.10	3.28	4.68	3.15	3.27	3.20	3.90	2.40	2.60	3.70
Na2O	4.15	3.10	3.28	4.68	3.15	3.14	3.90	3.50	3.30	3.60	3.60
K2O	3.22	3.37	3.43	3.25	3.44	3.46	PR2	PR3	PR4	PR5	PR6
P2O5	3.72	4.56	4.25	3.82	4.42	4.34	4.30	4.70	4.60	4.70	4.30
Total	1.00	0.62	0.71	0.58	0.67	0.67	0.70	0.90	0.50	0.60	0.70
Ba	100.00	100.00	100.00	100.00	100.00	100.00	100.00	100.00	100.00	100.00	100.00
Rb	479.75	281.36	263.48	316.84	380.68	322.99	19.35	36.53	46.22	65.95	90.15
Sr	1249.02	876.94	791.12	1013.65	1167.3	1042.07	1144.8	1139.5	1333.66	1296.8	1272.90
Zr	738.15	680.59	636.42	778.23	813.23	787.94	681.43	768.38	609.26	809.27	770.63
Pb	29.41	15.51	29.91	23.74	17.15	17.75	26.88	37.12	71.88	36.95	28.86
Y	18.20	10.28	10.49	15.00	13.06	13.29	11.22	11.76	21.74	13.57	11.51
Nb	67.56	65.25	69.21	59.39	51.73	51.77	58.86	65.11	56.71	48.93	65.25
U	2.20	1.63	2.31	2.16	1.73	1.98	5.15	1.74	1.80	6.68	3.21
Th	24.10	21.82	23.60	26.13	19.55	20.08	33.32	25.84	21.74	35.72	12.59

Table 3. Representative rare earth elementdata of volcanic rocks and pyroclastic deposits from Damavand volcano.

Sample	S4N4F	S4N4Li	S4N3ASH	S5N2F	S3N2AS	S3N2F	S3N3C	S3N3M	S3N3F	S3N3Li	S3N4C	S1R1	PR2	PR3	PR4	PR5	PR6
La	80.69	73.25	43.35	74.60	70.95	76.29	87.89	90.45	98.80	92.20	82.44	62.33	28.34	36.73	61.74	54.50	44.92
Ce	116.69	125.58	120.03	98.02	67.59	100.47	105.67	169.71	75.40	51.42	63.38	62.36	48.31	70.96	140.98	99.40	78.63
Pr	11.40	10.89	7.96	11.66	9.67	14.12	13.79	13.83	13.79	13.06	12.44	10.22	7.98	8.39	11.24	9.97	9.10
Nd	67.78	61.47	57.94	36.06	56.04	47.38	52.64	64.36	73.19	66.33	61.35	61.10	32.12	36.47	57.11	48.25	36.46
Sm	7.16	6.44	6.17	4.13	5.36	4.96	5.76	6.46	7.08	6.92	5.91	5.92	3.28	4.30	6.38	5.77	4.36
Eu	2.22	1.93	1.88	1.07	1.69	1.52	1.60	1.97	2.27	2.37	2.18	1.66	1.01	1.02	2.03	1.59	1.21
Gd	2.53	2.58	2.47	1.70	2.08	1.78	2.13	2.37	2.44	2.65	2.42	2.53	2.24	2.24	2.60	2.40	2.28
Tb	1.66	1.72	1.67	1.28	1.26	1.47	1.20	1.55	1.61	1.59	1.51	1.34	1.47	1.45	1.51	1.57	1.39
Dy	1.48	3.12	2.66	1.66	3.24	2.96	4.00	4.03	4.62	4.72	4.29	1.66	1.17	1.18	4.72	1.80	1.06
Ho	0.59	0.59	0.55	0.44	0.66	0.45	0.94	0.77	0.78	0.69	0.67	0.59	0.62	0.57	0.63	0.58	0.64
Er	2.45	2.56	2.34	1.72	1.75	2.02	1.73	2.21	2.30	2.37	2.36	2.45	1.95	2.06	2.47	2.34	1.94
Tm	0.21	0.22	0.20	0.14	0.17	0.14	0.18	0.19	0.19	0.22	0.20	0.21	0.19	0.18	0.21	0.20	0.19
Yb	1.95	1.87	1.68	1.46	1.64	1.78	1.83	1.94	1.94	1.98	1.98	1.95	1.51	1.55	2.13	1.75	1.65
Lu	0.17	0.18	0.17	0.12	0.14	0.12	0.14	0.16	0.16	0.18	0.16	0.17	0.15	0.15	0.17	0.16	0.16

Sample	S1N8M	S1N8F	S1N8Li	S2N2C	S2N2M	S2N2F	S2N2Li	S2N1ASH	S3N4M	S3N4F	S4N4C	S4N4M	S2R5	S2R6	S2R7	PR1	S2R2C
La	61.67	47.10	61.01	86.68	89.16	91.09	73.25	89.34	85.83	75.77	75.77	100.85	38.78	30.34	35.52	37.77	58.36
Ce	125.95	94.32	124.87	174.40	184.97	177.45	147.96	175.14	164.37	148.71	148.71	208.52	75.40	51.42	63.38	62.36	116.90
Pr	10.57	8.75	11.10	15.07	14.07	13.50	10.89	13.07	12.15	11.77	11.77	13.24	8.73	8.49	8.34	8.51	9.74
Nd	51.17	44.62	50.39	65.47	65.82	64.99	57.94	57.19	60.64	59.06	59.06	67.78	41.52	35.42	33.84	34.83	48.36
Sm	5.27	5.13	6.13	7.21	6.64	6.71	6.17	5.66	5.59	5.51	5.51	7.16	4.53	3.98	4.05	3.50	5.14
Eu	1.65	1.42	1.90	2.00	2.28	1.99	1.88	1.58	1.67	1.66	1.66	2.22	1.11	1.08	1.09	1.01	1.62
Gd	2.57	2.39	2.76	2.42	2.48	2.40	2.47	1.88	2.14	2.17	2.17	2.53	2.36	2.42	2.23	2.15	2.18
Tb	1.62	1.49	1.69	1.52	1.58	1.66	1.67	1.59	1.32	1.33	1.33	1.66	1.55	1.59	1.33	1.02	1.42
Dy	2.23	2.79	3.36	3.77	3.95	4.19	2.66	3.44	3.70	2.79	2.79	1.48	2.13	1.38	1.36	1.69	2.84
Ho	0.57	0.54	0.61	0.94	0.76	0.66	0.55	0.73	0.64	0.63	0.63	0.59	0.59	0.62	0.59	0.62	0.55
Er	2.40	2.11	2.61	2.25	2.19	2.24	2.34	2.16	1.94	1.93	1.93	2.45	2.12	2.05	2.02	1.41	2.21
Tm	0.22	0.21	0.22	0.21	0.19	0.19	0.20	0.15	0.18	0.18	0.18	0.21	0.19	0.21	0.19	0.18	0.18
Yb	2.00	1.88	2.09	1.80	1.87	1.80	1.68	1.43	1.71	1.88	1.88	1.95	1.74	1.62	1.70	1.51	1.70
Lu	0.18	0.17	0.19	0.16	0.17	0.16	0.17	0.12	0.14	0.15	0.15	0.17	0.16	0.17	0.16	0.15	0.15

Dy, Ho) and *HREE* (Er, Tm, Yb, Lu) [Fig.9 b & c]. Rayneh and Karam-Poshteh Pyroclastic deposits are enriched in Tb, but is notable depleted in Gd and Lu compared to Malar pyroclastic deposits.

The trace element data of volcanic rocks and pyroclastic deposit samples are plotted versus SiO_2 and against one another [Fig. 10]. Incompatible *LILE* (Rb, Ba and Sr) together with Th have not shown broad enrichment as a function of increasing SiO_2 content. However there is considerable variation in the concentrations of these elements at a given value of SiO_2, particularly Rb, Ba, Th and Zr. Pyroclastic deposits plots as a distinct cluster in comparison with volcanic rocks. Pyroclastic deposits are enriched in Rb, Ba Th, Zn and Zr in comparison to the volcanic rocks. Mallar pyroclastic deposits as the youngest explosive eruptions has the highest content of the above elements in comparison to the Rayneh and Karam-Poshteh pyroclastic deposits [Fig. 10]. Ce, Sr and Y show considerable scatter.

Zr data show two distinct groups for volcanic rocks and pyroclastic deposits. Volcanic rocks with the majority having high Zr with 100 to 300 ppm and the pyroclastic deposits have Zr contents which are intermediate between 500 to 900 ppm.

A comparison between geochemistry of the volcanic rocks and pyroclastic deposits show that the geochemistry can be contrasted. *LREE* (La, Ce, Hf, Pr) show scattered variations with SiO_2. Damavand pyroclastic deposits are typically enriched in *LREE* but show a large range in *LREE*. Mallar deposits as the youngest pyroclastic phase of Damavand is anomalously enriched in *LREE* (with the exception of Pr) compared to Karam-Poshteh and Rayneh pyroclastic deposits. The same trend can be observed with *MREE* (with the exception of Tb). In both trace element categories (*LILE* and *LREE*) the Mallar pyroclastic deposits with few minor exceptions shows the most enrichment.

Results and Discussion

Variations in the Major and trace element compositions of Damavand rocks and pyroclastic deposits are difficult to explain by fractional crystallization mechanism. An interesting observation is that K and Rb are well correlated only in Mallar pyroclastic deposits [Fig. 10]. The only major phase that might discriminate between K and Rb is biotite and the variations are consistent with K being significantly more compatible than Rb [16]. Zr data [Fig. 10] show that there are two groups of pyroclastic deposits with high Zr content (600 to 900 ppm in given SiO_2 content of 60%) and volcanic rocks as a low Zr group (100 to 300 ppm in given SiO_2 content of 60%). Scatter of several trace elements in plots against SiO_2 and incompatible trace elements (Zn, Ba, Th, Ce and Sr), also suggests that the petrogenesis is more complex than a simple fractionation process from a single composition parent. High K, Ba and Rb content in both volcanic rocks and pyroclastic deposits could be due to enrichment of these elements in the source. Rb, Ba may be accepted in the plagioclase and biotite which have structures large enough to accommodate Ba [9].

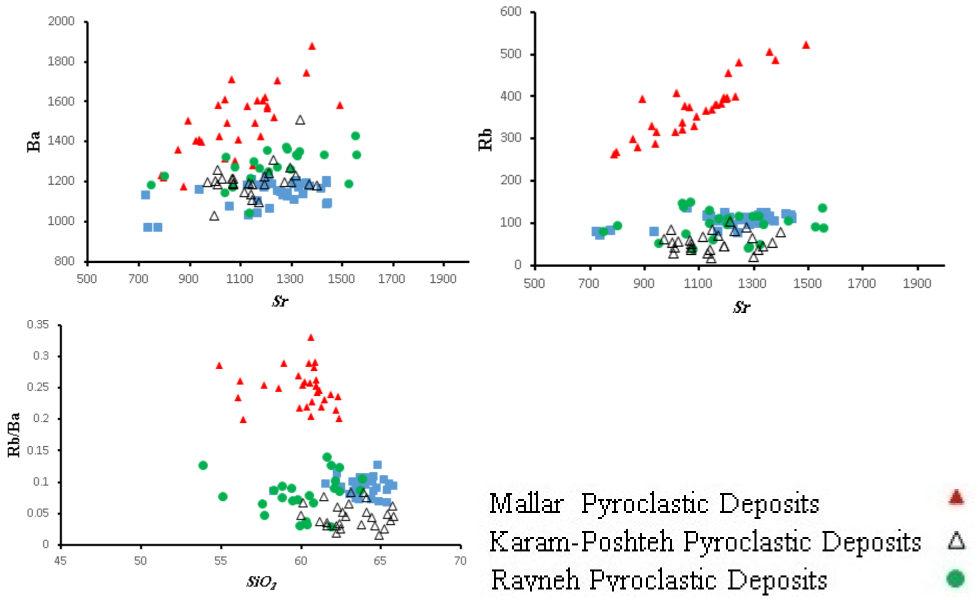

Figure 10. Trace elements variation diagrams for pyroclastic deposits of Damavand Volcano. Symbols are the same as Fig.15.

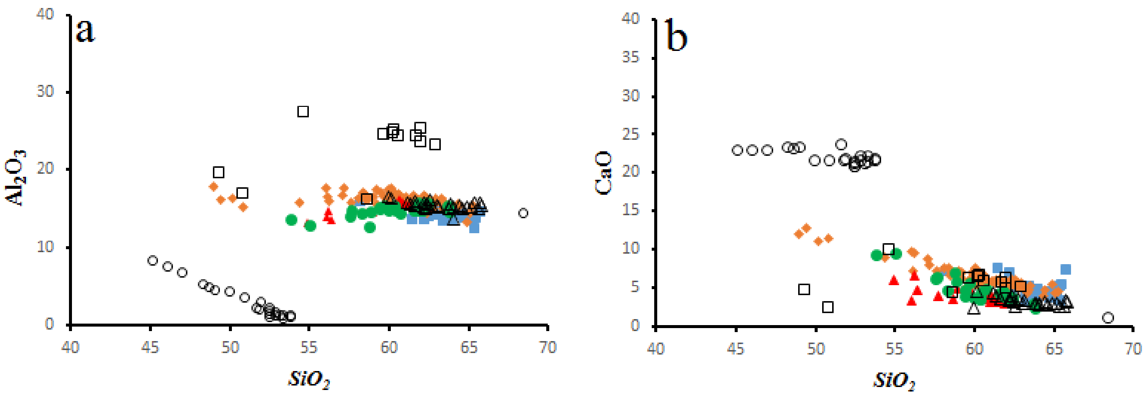

Figure 11. Variation diagrams of lavas and pyroclastic deposits compositions (plotted as the same symbols as Fig. 7) to illustrate possible magma evolution by crystal fractionation. Al_2O_3 (a), CaO (b) are plotted against SiO_2. Compositions of the main crystal phases are plotted: plagioclase (open squares) and pyroxene (open circles).Other symbols are as the as Fig.7.

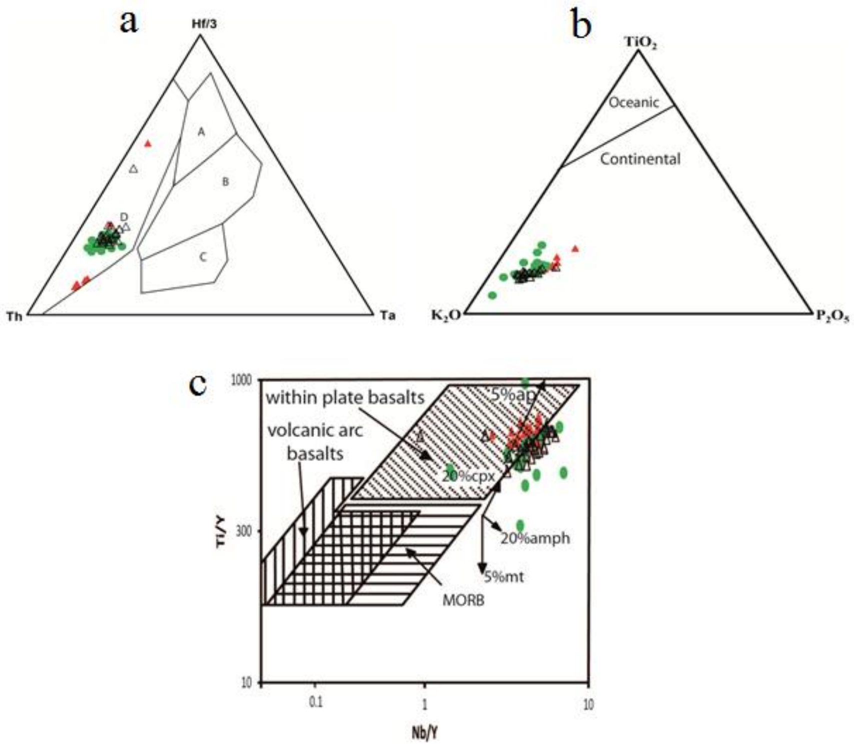

Figure 12. Geochemical affinity of Damavand pyroclastic deposits. (a): Hf-Th-Ta triangular diagram *after* [19], (b): K_2O-TiO_2-P_2O_5 triangular diagram, (c): Ti/Y vs. Nb/Y discriminant diagram *after* [14], with effects of fractionation of modal phases; ap: apatite, cpx: clinopyroxene, MT: magnetite and amp: amphibole.

Diagrams of mineral composition are used to test whether fractionational crystallization might have evolved. Al_2O_3 and CaO content in, plagioclase and pyroxene and bulk composition of whole rock were plotted against SiO_2 [Fig. 11a & b]. The trend suggest that evolution of trachyandesitic lavas and pyroclastic deposits might not be explained by simple fractionation but there is not enough mineral composition data available on Damavand lavas and pyroclastic deposits.

Tectonic-environment diagrams are only valid for primitive rocks, and the Damavand rocks are highly differentiated. Relatively high Th and Low Y contents can be intemperate as crustal contamination. Differentiation and contamination processes of Damavand rocks make uncertainty about the plotting areas in the above discriminant diagrams. Presence of magnetite and apatite imply fractionation processes have been involved and is responsible for considerable scatter in trace element characteristics. Fractionation vectors [Fig. 12 a, b and c] suggest that parental magmas probably had lower Nb/Y ratios, while providing little constraint on parental Ti/Y ratios. *Davidson et al (2004)*[4] show that basalts from the region, which might represent parental magmas, do have lower Nb/Y ratios and plot closer to the within-plate fields.

Volcanic rocks and pyroclastic deposits contain high Nb content (50-80) which is much higher than sebduction related magma and volcanic arc rocks. Geochemistry data also show no apparent trends through time and distinct similarity can be observed between Damavand trachyandesits with the same rocks from interaplate magma setting. Field observation such as limitation of magmatism in region suggest that decompression melting and local hotspot formation could be investigate in Damavand.

Acknoladgments

The author would like to thank Steve Sparks for his very useful comments. The research was partly funded by Ministry of Sciences, Research and Technology of Iran.

References

1. Allenbach P. Geologie und petrologie des Damavand und seiner umgeurg (Zentral-Elburz), Iran.*Phd.Theses*. Geologisches Institut, ETH Zurich, Mittellung**. 63**, 114p. (1963).
2. Allenbach P. Geology and Petrography of Damavand and its environment (Central Alborz), Iran, *Geological Survey*

of Iran Report, 27p. (1970).
3. Darvishzadeh A., and Mordi M. Fall differentiation in pyroclastic fall deposits of Damavand Volcano. *Journal of Science(Persian)*, **23** (1): 31-46 (1997) .
4. Davidson J., Hassanzadeh J., Stockli D.F., Bashukooh B., Turrin B., and Panamouz A. The geology of Damavand volcano, Alborz Mountains, northern Iran. *GSA Bulletin* **116** (1): 16-29 (2004).
5. Emami M.H. Damavand Volcano and its Probable Activity. *Geological Survey of Iran*, 559 p. (1989).
6. Galland O., Hallot E., Cobbold P.R., Ruffet G., and Bremond d'Ars J. Volcanism in a compressional Andean setting: a structural and geochronological study of Tromen volcano (Nequen Province, Argentina). *Tectonics*, **26** (4): 1-24 (2007).
7. Gill j. B. Orogenic Andesite and Plate Tectonics. Springer, Berlin, Heidelberg, 87p. (1981).
8. Jackson J., Priestley K., Allen M., and Berberian M. Active Tectonics of the South Caspian Basin. *J. Geophys. Res,* **148** (2): 214-245 (2002).
9. Mason B., and Moore C.B. The structure and composition of the Earth. *Principles of geochemistry*, 344p. (1982).
10. Miyashiro A. Volcanic rock series in island arcs and active continental margins. *Earth Sci. Rev*, **274** (4): 321-355 (1974).
11. Mohamadi L. Petrography, Geochemistry and Petrogenesis of the Youngest lava of Damavand Volcano, *MSc. Theses*, Earth Sciences Research Center, 132p. (2016).
12. Mortazavi M., Sparks R.S.J. and Amigo A. Evidence for Recent Large Magnitude Explosive Eruptions at Damavand Volcano, Iran with Implications for Volcanic Hazards, *J.Sci.I.R.Iran* **20** (3): 253-264 (2009).
13. Mortazavi M. The Youngest Pyroclastic Activity of Damavand Volcano, an Example of Sub-Pillinian Eruption with Stratospheric Level of Volcanic Plum. *Geo.Sci* **23** (89): 155-164 (2013).
14. Pearce J.A. Role of sub-continental lithosphere in magma genesis at active continental margins. In: continental basalts and mantle xenoliths, *Springer*, Berlin, 230-249 (1982).
15. Peccerillo A., and Taylor S. R. Geochemistry of Eocene calc alkali volcanic rock from the Pegues L'abbe. *Contrib. mineral. Petr.***58** (1): 63-81 (1976).
16. Sisson T. W. Hornblende-melt trace-element partitioning measured by ion microprobe. *Chem. Geol***, 117** (1): 331-344 (1994).
17. Sun S. and McDonough W. Chemical and isotopic systematic of oceanic basalts: Implication for mantle composition and processes. *Geol. Soc,* **42** (1): 313-345 (1989).
18. Tatar M., Jackson J., Hatzfeld D., and Bergmen E. The 2004, May 28 Beladeh earthquake (M*w* 6.2) in the Alborz, Iran: overthrusting the South Caspian Basin margin, partitioning of oblique convergence, and seismic hazard of Tehran. *J. Geophys. Res,* **170** (1): 249-261 (2007).
19. Wood D. A. The application of a Th Hf Ta diagram to problems of tectonomagmatic classification and to establishing the nature of crustal contamination of basaltic lavas of the British Tertiary volcanic province. *Earth Planet. Sci. Lett,* **50** (1): 11-30 (1980).